Paper 3:

Interpretation of Ion Velocity Distributions Measured with a Grounded Retarding Field Energy Analyzer (RFEA) in an Inductively Coupled Helicon Plasma

N. Gulbrandsen, W. J. Miloch, and Å. Fredriksen, *Contributions to Plasma Physics*, **53**, 27, (2013), doi: 10.1002/ctpp.201310005.

Contrib. Plasma Phys. **53**, No. 1, 27 – 32 (2013) / **DOI** 10.1002/ctpp.201310005

Interpretation of Ion Velocity Distributions Measured with a Grounded Retarding Field Energy Analyzer (RFEA) in an Inductively Coupled Helicon Plasma

N. Gulbrandsen*, **W. J. Miloch****, and **Å. Fredriksen**

Department of Physics and Technology, University of Tromsø, N-9037 Tromsø, Norway

Received 02 December 2011, revised 09 April 2012, accepted 01 October 2012
Published online 09 January 2013

Key words Retarding field energy analyzer, ion temperature, sheath.

A Retarding Field Energy Analyzer (RFEA) with a grounded surface in a plasma will be surrounded by a sheath. The ion distribution function (IDF) measured at the probe will be distorted as compared to the IDF in a plasma unaffected by the sheath.
In the present study we investigate whether a practical method can relate the measured distribution function to the undisturbed IDF, thus allowing for derivation of useful plasma parameters from the measured IDFs.
We study the IDF in the sheath by 3D numerical simulations of a spherical RFEA for parameters similar to the Njord helicon device at the University of Tromsø. By comparison with the numerical results, we critically assess the results from simple 1D models that are often used in the analysis of the RFEA signal. With the PIC simulations we also show that the acceptance angle of the probe has a significant effect on the low energy part of the measured IDF. This result is compared with real probe measurements from the Njord device.

1 Introduction

A Retarding Field Energy Analyzer (RFEA) is a standard tool for measuring the ion distribution function (IDF) in a plasma. The RFEA probe usually consists of a small aperture opening and two or more grids that can be biased at different voltages to prevent electrons from entering and to repel ions below certain velocities, and a collector to measure the ion current [1]. If the probe surface is grounded in an electropositive plasma, a sheath with a voltage drop of approximately the plasma potential will form in front of it. This sheath will affect the IDF measured at the probe. Thus, to study the IDF in the plasma undisturbed by the sheath, one needs to find the way to relate the IDF at the probe to that in the plasma. The method might depend on the parameters of the plasma in question. In this study we critically assess different models for the IDF in the sheath that are often used in the analysis of RFEA data [2, 3]. We consider parameters similar to the plasma in the Njord device [4] at the University of Tromsø. This is a helicon plasma source running in an inductively coupled mode with a weakly magnetized plasma.

2 Methods

2.1 Numerical simulation

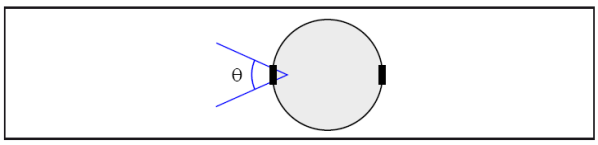

Fig. 1 A spherical probe with orifice (in black) and the acceptance angle (θ). A spherical probe is used for the simulation to simplify calculations. The RFEA used in the experiments has a rectangular shape.

* Corresponding author. E-mail: njal.gulbrandsen@uit.no
** Now at Department of Physics, University of Oslo, Norway

To investigate the evolution of the IDF from the undisturbed bulk plasma and through the sheath we have carried out 3D particle-in-cell (PIC) simulations plasma around a RFEA-probe [5, 6]. In the simulations, the sheath around RFEA forms self-consistently. The simulation was done for a plasma density of $n = 2.5 \cdot 10^{16}$ m^{-3}, $T_e = 4$ eV and $T_i = 0.4$ eV. For the studies of the acceptance angle, a potential drop from plasma to the probe of 45 V was used. The aperture opening of the probe would limit the velocity directions of ions entering the probe to a cone with a given acceptance angle. Figure 1 shows a schematic drawing of the probe with the acceptance angle. For the simulation of the IDF in the sheath potential drops of 18 V, 40 V and 95 V where used. 18 V would be close to the floating potential in this simulation. A more thorough description of the simulation is given in [5–7].

2.2 Analytical models

Models that relate the IDF at the RFEA surface to that in the plasma undisturbed by the sheath of the probe has to include simplifying assumptions relative to more complete sheath models [8]. Often, there is a need for a simple expression that could be fitted to the data. The models investigated here are one-dimension al and we assume that the ion distribution in the plasma is Maxwellian.

The current to the collector in an RFEA is usually taken as [1, 2, 9]:

$$I(v) = A_p e \int_{v_0}^{\infty} v f(v) dv \tag{1}$$

where A_p is a constant depending on the front-plate aperture and the analyzers transmission factor and $f(v)$ is the ion velocity distribution at the probe surface. The minimum velocity, v_0, relates to the discriminator voltages V as $v_0 = \sqrt{2eV/m_i}$, where m_i is the ion mass. Solving this for $f(v)$ we find that the IDF is proportional to the derivative of the collector current with respect to the discriminator voltage, $f(v) = \frac{m_i}{A_p e^2} \frac{dI(V)}{dV}$ [1, 10]. A common method to infer a temperature from an RFEA-measurement is to use the expression [2]:

$$kT_i = \frac{e}{\frac{d}{dV} \ln\left(\frac{I(V)}{I_0}\right)} \tag{2}$$

where $I(V)$ is the measured ion current as a function of discriminator voltage and I_0 is the ion saturation current. This expression implies that the distribution is Maxwellian or a truncated Maxwellian, at least for the part of the distribution where $v > \sqrt{2eV_p/m_i}$. This can be achieved by assuming that the plasma is completely collisionless and that the sheath works as a simple potential drop accelerating every single particle [11, 12]. The particles then gain an energy of $e\Delta V$, where ΔV is the potential drop. If the particle goes through the whole sheath, ΔV equals the plasma potential V_p between the bulk plasma and the grounded probe. This model only accounts for particles that are already moving toward the probe. The velocity at the probe would be given as $v = \sqrt{v_s^2 + \frac{2e\Delta V}{m_i}}$ for $v_s > 0$, v_s is the velocity at the sheath edge and m_i is the ion mass. It is assumed that all particles experience the same potential drop. The ion velocity distribution function is then [12]:

$$f(v) = A \exp\left(-\frac{m_i\left(v^2 - \frac{2e\Delta V}{m_i}\right)}{2kT_i}\right) \quad \text{for} \quad v^2 > \frac{2e\Delta V}{m_i} \tag{3}$$

where A is a normalization constant and T_i is the ion temperature. In figure (2, a and b) this function is plotted for different values of ΔV representing different positions in the sheath. Here $\Delta V = 0$ refers to the potential in the bulk plasma and V is the discriminator voltage needed to repel ions with this velocity.

In figure 2 a) and b) we have also plotted the analytical solution of Emmert's sheath model [13], a more sophisticated 1D-model that also accounts for the presheath. From the figure we can see that the right hand side of Emmert's model coincides with a truncated Maxwellian. We therefore argue that using the approximation of a truncated Maxwellian to analyze RFEA-measurements would give the same derived temperature as Emmert's model as long as we analyze only the right hand side of the distribution.

A different approach would be to assume that the plasma is collisional in the sheath. The distribution would then approach a drifting Maxwellian [2, 11, 12]. This is also the analysis that one would use for a flow or a beam

in a plasma [14]. The velocity at the probe is then given as $v = v_s + v_f$ where v_f is the flow velocity [3]. To analyze this we have to assume that the ion velocity distribution at the probe is a shifted Maxwellian distribution:

$$f(v) = A \exp\left(-\frac{m_i(v - v_f)^2}{2kT_i}\right) \tag{4}$$

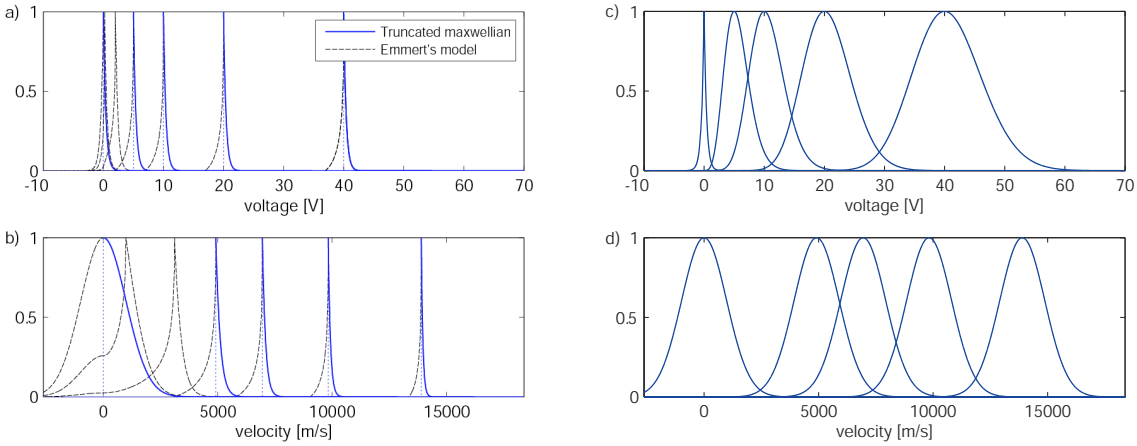

Fig. 2 Comparison of theoretical ion distribution functions (IDF's) for particles accelerated in electric potential, (a) and (b), and distribution with a bulk velocity, (c) and (d). (a) and (c) shows the distributions plotted with regards to discriminator voltage while (b) and (d) is plotted with regard to velocity. The distributions are plotted at the potential drop ΔV of 0 V, 5.63 V, 11.25 V, 22.5 V and 45 V, and the corresponding bulk velocities 0 m/s, 520.93 m/s, 736.7 m/s, 1041.9 m/s and 1473.4 m/s. Emmert's model is plotted for two additional positions, one in the preasheath and one at the sheath edge. For all cases the start distribution is taken as a Maxwellian ion distribution of argon with temperature of 0.4 eV. All distributions are normalized to a maximum height of 1

In figure 2 c) and d) a shifted Maxwellian is plotted for flow velocities corresponding to the peak values from the distribution in figure 2 a) and b) and with a temperature of 0.4 eV. If $V = \frac{1}{2}\frac{m_i v^2}{e}$ and we relate the flow velocity to the total potential drop as $V_p = \frac{1}{2}\frac{m_i v_f^2}{e}$ we can find a temperature estimate:

$$kT_i = \frac{e}{\frac{d}{dV_s}\ln\left(\frac{I(V_s)}{I_0}\right)} \qquad \text{where} \quad V_s = \left(\sqrt{V} - \sqrt{V_p}\right)^2 \tag{5}$$

3 Results

3.1 Effect of the acceptance angle

θ	kT_i [eV]	Shifted kT_i [eV]
10°	3.52 ± 0.07	0.28 ± 0.01
20°	3.5 ± 0.1	0.30 ± 0.01
45°	3.6 ± 0.1	0.33 ± 0.02
90°	3.7 ± 0.1	0.35 ± 0.02

Table 1 Temperatures of the distributions in figure 3 calculated assuming truncated Maxwellian and shifted Maxwellian.

As it can be seen from figure 3, showing results from PIC simulations, the acceptance angle strongly affects the left hand side of the distribution while the right hand side seems to be preserved. The distributions have been normalized to a maximum height of unity since the amount of particles entering the orifice changes with the acceptance angle. The position of the maximum of the distribution seems not to be affected by the acceptance angle, although it is slightly below $\Delta V = 45$V that was chosen to be the potential drop. Applying equation (2) we can find a measure of the temperature of the distribution. The results for the distributions shown in figure 4

are given in Table 1 together with the the estimated temperature assuming shifted Maxwellian. The uncertainties are derived from the accuracies of the linear fit to the logarithm of the integrated IDF.

Figure 4 shows laboratory measurements of IDFs from two different RFEAs with different acceptance angles. In a) we have a large acceptance angle of about $100°$ and we can clearly see a low velocity tail in the measured IDF. This tail is not visible in b) where the acceptance angle is around $45°$. The tail in 4 a) is much longer than in the results from the PIC simulation (see again figure 3).

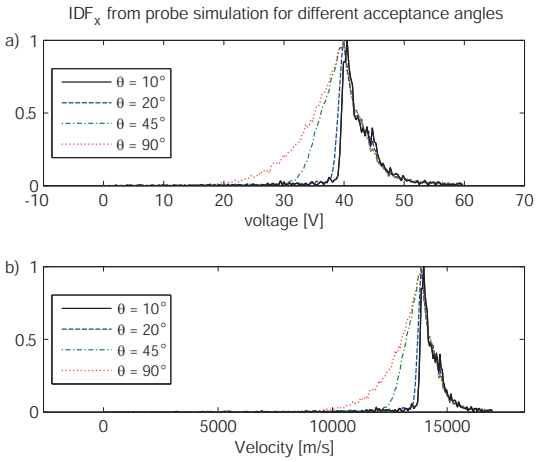

Fig. 3 Distributions registered at the simulated probe for different acceptance angles with a 45 V potential drop in the sheath.

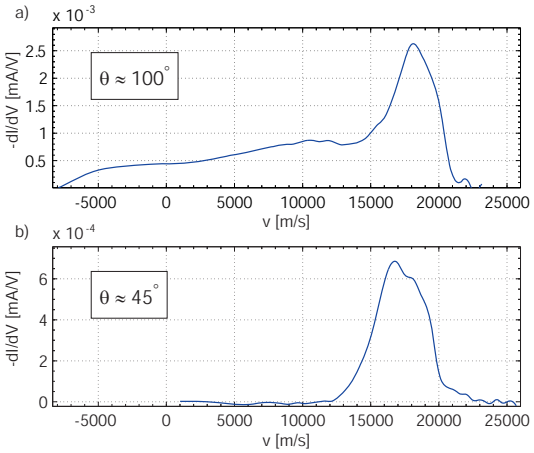

Fig. 4 Measurements of IVD's done with two different RFEA. One with $\sim$ $45°$ acceptance angle and one with $\sim$ $100°$ acceptance angle. The measurements are done in similar plasma condition at the same position in the plasma. RF power: 500 W, Gas pressure: $P = 27$ mPa Argon, Magnetic field $B \sim 3$ mT, Electron density $n_e \sim 2 \cdot 10^{16}$ m^{-3}. Both probes have grounded surface and front grid.

3.2 IDF in the sheath

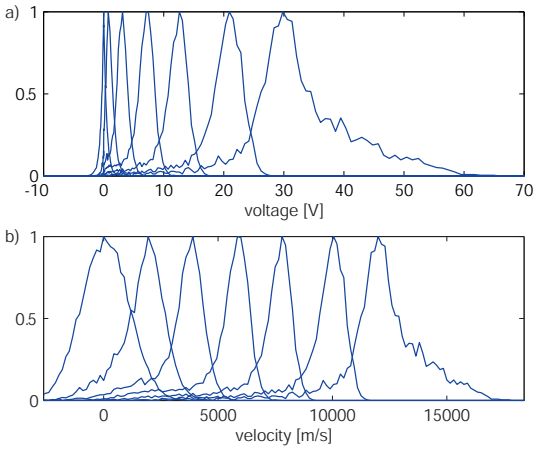

Fig. 5 Radial ion distribution functions in the bulk plasma and different positions in the sheath from the PIC simulation with a voltage drop of 40 V in the sheath, averaged over a spherical shell with radial distance $r_i < r < (r_i + \delta r)$ where $\delta r = 0.084\,\lambda_{De}$.

Figure 5 shows a collection of radial IDFs (directed toward the grounded probe) obtained from the PIC simulations, taken at different positions in the the sheath and presheath. The distributions are derived by averaging over a spherical shell with radial distance $r_i < r < (r_i + \delta r)$ where $\delta r = 0.084\,\lambda_{De}$. Closest to the probe the distributions become noisy due to low number of particles and large potential gradient. The distributions are plotted as a function of voltage, a) and velocity, b) for comparison with models and probe measurements. The voltage is calculated as $V = \frac{1}{2}\frac{m_i v^2}{e}$. All distributions are normalized to a maximum height of unity.

From the IDFs we can derive characteristic parameters that can be compared with analytical models. In figure 6 we have plotted these parameters for three sheath voltages and the corresponding parameters for Emmert's model and the shifted Maxwellian.

Here Emmert's model was chosen instead of the truncated Maxwellian because it is able to generate a low energy tail that we also see in our simulation. The behavior of these to models is otherwise similar.

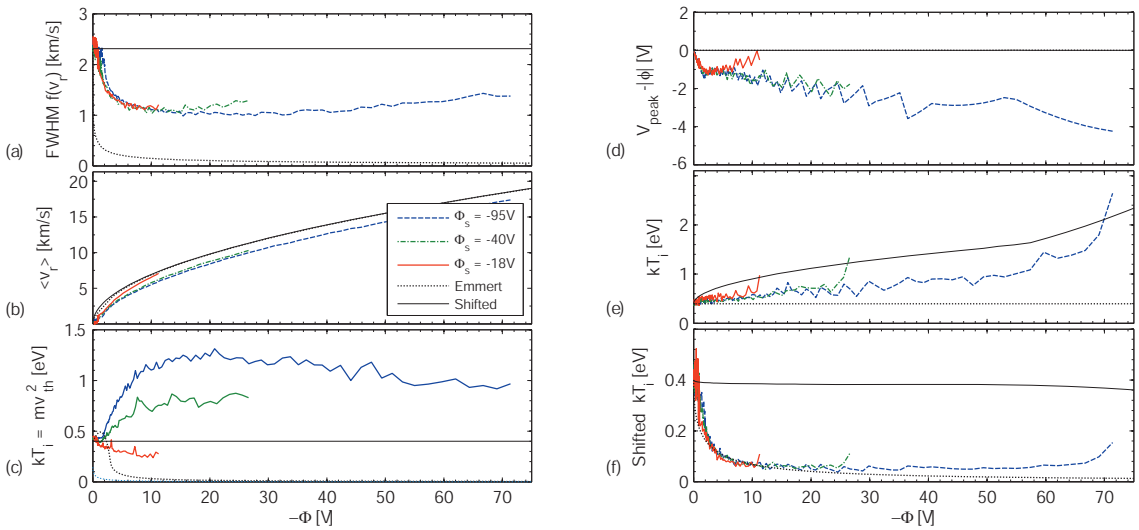

Fig. 6 (a) Full width half maximum, (b) Mean velocity, (c) Thermal velocity calculated as the standard deviation of the distribution, (d) Peak of distribution relative to local potential, (e) Temperature measured from a linear fit to the logarithm of the integrated distribution. (f) Temperature measured from a linear fit to the logarithm, assuming shifted Maxwellian.

In figure 6 a) we see how the full width half maximum (fwhm) of the radial ion velocity distribution changes as a function of local potential in the sheath. The fwhm of the simulated IDFs drops to about half of the original width before they slowly starts to rise again. This slow increase of fwhm in the inner part of the sheath seems to depend on the total voltage across the sheath. The shifted Maxwellian keeps it's fwhm for all voltages while the distribution functon from Emmert's model falls off much faster than the simulations, and eventually goes toward zero. Figure 6 b) shows the average radial velocity of the distribution.

In figure (6 c) we have calculated the variance of the distribution in units of energy as a measure of temperature, $m_i\sigma^2 = m_i v_{th}^2 = m_i \cdot \frac{\sum (v-\overline{v})^2 f(v)}{\sum f(v)}$ where the thermal velocity, $v_{\rm th}$ would be the standard deviation of the distribution. For the simulations with potential drop of 40 V and 95 V the variance increases in the first part of the sheath. This increase is probably due to the long tail that develops at lower velocities in these simulations. For the simulation with 18 V potential drop, the variance is slightly reduced while for Emmert's model the variance increase slightly in the presheath before it drops quickly in the sheath.

Figure 6 d) shows a plot of the position of the peak of the distribution in voltage relative to the local potential. The peak position in voltage is always at the local potential for all these 1D models, but in the simulation data we see that the peak potential is slightly lower than the local potential.

For the 95 V sheath the peak of the measured distribution at the probe can be as much as 4 V less than the sheath potential drop that is usually interpreted as the plasma potential [14].

In figure 6 e) we have derived the temperature from Eq. (2) by doing a linear fit to the logarithm of the current. Emmert's model and the truncated Maxwellian will then give a constant temperature indicating that this is the correct method to analyze these models, while the shifted Maxwellian increases in the sheath. The simulation results lies somewhere in between Emmert's model, (and thereby the truncated Maxwellian), and the shifted Maxwellian. The accuracy of the fit is within 0.15 eV.

In figure 6 f) we have assumed a shifted Maxwellian and done a linear fit to the logarithm of the shifted current (Eq. 5). The shifted Maxwellian gives here close to a constant value, while Emmert's model drops off quickly. The simulation results are in this case closer to Emmert's model than the shifted Maxwellian although they seem to deviate slightly in the inner part of the sheath. The accuracy of the fit is within 0.08 eV.

4 Discussion and conclusion

From figures 3 and 2 we can infer that the model of acceleration through a potential figure, 2 a) and b), does not look like a good model for the simulated plasma. Using this model to analyze the data gives a much too high temperature estimate (table 1). From these figures the simulation looks much closer to a shifted Maxwellian figure 2 c) and d), but with a lower temperature than the background plasma. Looking at the derived temperatures in figure 6 f) we see that the assumption of a shifted Maxwellian gives much too low temperature estimate for the distributions in the sheath. When the same procedure is applied to the simulated probe measurements (figure 4) the derived temperature is closer to the initial temperature, and significantly higher than in the middle of the sheath. We have no good explanation for this discrepancy between the distribution in the middle of the sheath and at the probe. Due to few ions and steep potential gradient we where not able to retrieve good distributions from the innermost part of the sheath. In our data (figure 6) we see an increase in the estimated temperatures for both methods in the inner part of the sheath. If this is a real effect or just an artifact of averaging over a too large part of the sheath is not known. Together with the slight increase of fwhm in the inner part of the sheath this could indicate a geometric effect due to a finite probe in a 3-dimensional plasma.

Assuming a truncated Maxwellian, Buzzi et. al. [11] and Anderson et al. [12] also reported too high temperature estimates in a magnetized cesium plasma when the densities were above $5 \cdot 10^8$ cm^{-3}. They attribute this to ion-ion collisions altering the direction of the particle trajectories so that energy from the two remaining dimensions is spread into the radial direction. They both concluded that the distribution would go toward a drifting Maxwellian with temperature of $\frac{2}{3}$ of the original temperature.

In our simulations we have no explicit collisions included, but electrostatic forces between the particles could result in fluctuations in the potential that might alter the particle trajectories. Still the decrease in temperature in the sheath we see in the simulation is much more than $\frac{1}{3}$. The fwhm decrease to about $\frac{1}{2}$ of the original figure 6 a) and the temperature estimate for assuming shifted Maxwellian drops to about $\frac{1}{4}$ (figure 6 f). This might indicate that we are somewhere in-between those two regimes and that there might be some weak ion-ion collisions in the sheath.

By performing PIC simulations, we found that the acceptance angle of the probe affects the left side of the measured IDF, while the right side and the maximum are not affected by the acceptance angle. The peak of the distribution seems to follow after the plasma potential with a few volt. By comparison with simulations we critically assessed the results from simple 1D models that are often used in the analysis of the RFEA signal. We found that the simple method of deriving the temperature from RFEA-measurements assuming a collisionless 1-dimensional plasma is not appropriate for our conditions. The simulated IDFs in the sheath are somewhat in-between a drifting Maxwellian and a simple acceleration in a potential drop. This indicates that the sheath in front of a grounded RFEA in the plasma parameter regime of our device is affected by collisions. Hence, collisionless models to derive T_i cannot be applied.

References

[1] C. Böhm and J. Perrin, Review of Scientific Instruments **64**, 31–44 (1993).
[2] E. Leal-Quiros and M.A. Prelas, Plasma Science, IEEE Transactions on **16**, 661–666 (1988).
[3] H.M. Küdyan, Review of Scientific Instruments **49**, 8–10 (1978).
[4] H.S. Byhring, C. Charles, Å. Fredriksen, and R.W. Boswell, Physics of Plasmas **15**, 102113 (2008).
[5] W.J. Miloch, N. Gulbrandsen, L.N. Mishra, and Å. Fredriksen, Applied Physics Letters **97**, 261501 (2010).
[6] W.J. Miloch, J. Trulsen, and H.L. Pécseli, Phys. Rev. E **77**, 056408 (2008).
[7] W.J. Miloch, N. Gulbrandsen, L.N. Mishra, and Å. Fredriksen, Physics of Plasmas **18**, 083502 (2011).
[8] P.C. Stangeby, The plasma boundary of magnetic fusion devices, Plasma physics series. (Institute of Physics Publishing, 2000).
[9] C. Charles, R.W. Boswell, and R.K. Porteous, Journal of Vacuum Science and Technology A: Vacuum, Surfaces, and Films **10**, 398–403 (1992).
[10] H. Ikezi and R.J. Taylor, Journal of Applied Physics **41**, 738–742 (1970).
[11] J.M. Buzzi, H.J. Doucet, and D. Gresillon, Physics of Fluids **13**, 3041–3049 (1970).
[12] S.A. Andersen, V.O. Jensen, P. Michelsen, and P. Nielsen, Physics of Fluids **14**, 728–736 (1971).
[13] G.A. Emmert, R.M. Wieland, A T. Mense, and J.N. Davidson, Physics of Fluids **23**, 803–812 (1980).
[14] Z. Harvey, S.C. Thakur, A. Hansen, R. Hardin, W.S. Przybysz, and E.E. Scime, Review of Scientific Instruments **79**, 10F314 (2008).

